ORIGINAL ARTICLE

Catalytic activity of Co (II)-porphyrin anchored onto polymeric support of electrospun polyacrylonitrile nanofiber: synthesis and efficient green oxidation of crystal violet dye with hydrogen peroxide

Sahar H. El-Khalafy[1] · Mohamed M. Azaam[2] · Esraa M. El-nshar[2,3] · Elbadawy A. Kamoun[4,5] · El-Refaie Kenawy[2]

Abstract

A novel method was explored in this study to address water contamination challenges by utilizing nanofiber mat-supported metalloporphyrin materials. Specifically, electrospinning was employed to create various compositions of polyacrylonitrile (PAN) mixed with different concentrations of Co(II) complex of tetrakis-5, 10, 15, 20 (4-hydroxyphenyl)porphyrin Co(II)TPHPP **1** anchored to chloroacetylated poly (*p*-hydroxy styrene) CAPS. These resulting nanofiber mat-supported metalloporphyrin materials were comprehensively analyzed using UV, FTIR spectrum, SEM, and TGA thermographs. The study found that the designed nanofibers acted as efficient catalysts for the oxidative breakdown of crystal violet (CV) dye using H_2O_2 in aqueous solutions. Among these materials, the nanofiber composed of a 1:1 ratio of PAN to Co(II)TPHPP/CAPS with a lower Co(II)TPHPP loading (NF6), demonstrated the highest catalytic activity, decomposing CV completely within 60 min. Various experiments were conducted to explore the effects of H_2O_2 concentration, catalyst dosage, and temperature on the catalytic degradation of CV with the NF6 nanofiber mat-supported metalloporphyrin. An interesting finding was the enhanced recovery and recyclability of the catalyst due to the immobilization of metalloporphyrin on chloroacetylated polymer-supported nanofiber mats. Remarkably, even after five cycles of reuse, there was no significant degradation in the catalytic activity of the recycled catalyst. This breakthrough highlights the potential of these materials in addressing water pollution challenges efficiently and sustainably.

Keywords Metalloporphyrins · Electrospinning · Nanofiber · Green oxidative degradation · Crystal violet

✉ Sahar H. El-Khalafy
saharelkhalafy401@gmail.com

✉ El-Refaie Kenawy
ekenawy@science.tanta.edu.eg

1 Department of Chemistry, Faculty of Science, University of Tanta, Tanta 31527, Egypt

2 Polymer Research Group, Department of Chemistry, Faculty of Science, University of Tanta, Tanta 31527, Egypt

3 Chemistry Department, Faculty of Dentistry, Sinai University, Kantara 41612, Egypt

4 Polymeric Materials Research Dep, Advanced Technology and New Materials Research Institute (ATNMRI), City of Scientific Research and Technological Applications (SRTA-City), New Borg Al-Arab City, Alexandria 21934, Egypt

5 Nanotechnology Research Center (NTRC), The British University in Egypt (BUE), El-Sherouk City, Cairo 11837, Egypt

1 Introduction

Nowadays, organic chemicals are generated in huge quantities by human activities, such as industrial and agricultural activities, that are widely discharged into the river water and increase pollution [1, 2]. These pollutants, including plasticizers, phenols, biphenyls, nitro and amine chemicals, organic dyes, insecticides, herbicides, and pesticides, are extremely harmful as they resist environmental conditions. Furthermore, they can harm the aquatic balance and the water portability [3, 4]. Dyes in wastewater impact the properties and quality of the H_2O by preventing sunlight penetration into the stream, reducing the response of photosynthetic [5]. Crystal violet (CV), one of the renowned cationic dyes, has a complex structure that makes removing it from wastewater difficult [6, 7], and poses severe risks to human health. Inhalation, ingestion, and skin absorption of CV dye can cause terrible rashes, acute eye inflammation, breathing issues, nausea, hypertension, painful sensitization, and kidney failure [8]. Despite these adverse effects, these cancer-causing

dyes are still produced and used in commerce. Currently, various conventional techniques are utilized like processes of physicochemical (i.e., solvent extraction, adsorption, reverse osmosis, ion exchange, coagulation, filtration, and chemical precipitation), bacterial, and fungus remedies were used in water treatment. However, they just transfer contaminants from water to another medium rather than totally destroying them; which frequently results in secondary contamination so they are non-destructive techniques [9, 10]. Among other pollutions management techniques, the utilization of advanced oxidative processes (AOP), such as photo-catalysis and Fenton reactions are being used more frequently to remove organic pollutants. Additionally, these techniques are focused on the decomposition of organic substances by unselective the reactive oxygen species (ROS) created by appropriate catalysts owing to their high qualification to oxidize the organic compounds to less hazardous molecules, such as H_2O and CO_2 [1, 11].

Metalloporphyrins are of great interest for use as activator catalysts for several oxidation reactions [12–16]. There are limited reports in the literature handling the degradation and destruction of organic dye application with transition metal complexes of homogenous porphyrins [17–20]. However, several difficulties are associated with using metalloporphyrins in homogeneous catalysis, including deactivation, poor recyclability, and recovery. Furthermore, porphyrin particles can aggregate in aqueous media depending on their structure, compromising their catalytic efficacy [21, 22]. To overcome the above limitations, immobilizing metalloporphyrins on solid supports (zeolites, hydrogels, microparticles, etc.) has led to remarkable activity in hybrid materials with high stability for easy removal and reuse [3, 23–32].

Fibrous electrospun mats are a novel way to reduce water pollution. Electrospinning is a quick and very flexible method that makes it possible to create continuous, one-dimensional micro/nanofibers with a lot of porosity. Surface area and customized mechanical developments were found to be very high to volume ratio. Effective carriers for the catalyst include electrospun mats made from several polymers [33–36]. The active catalyst particles can be attached on the outside surface and inside the nanofiber mat by electrospinning catalyst or catalyst precursor with a polymer matrix blend. The reactant can distribute on or inside the carrier during the reaction, and each active catalyst species has the potential to trigger a chemical reaction [34, 37]. Current research shows these nanofiber mats can remove and decompose organic dyes from water [34, 38]. Rahmat et al. studied the MnO_2 nanofibers' potential to aid in destroying crystal violet dye. The best conditions for photocatalytic reaction were applied in the presence of H_2O_2 at pH 3, with practically 97% dye degradation after 90 min of irradiation time [39]. Vinosel et al. used a hydrothermal technique to create varied ratios of Fe_3O_4/SnO_2 nanocomposites and investigate their photocatalytic activity on the organic pollutant crystal violet. The optimal ratio of Fe_3O_4/SnO_2 nanocomposites resulted in an

83% effective photocatalytic decomposition of CV dye under UV light irradiation [40]. Tavakoli et al. centered on creating $ZnTiO_3$-based perovskite nanoparticles to destroy Rhodamine B (R.B.) and crystal violet dye contaminants in sunlight. The remarkable photocatalytic activity of $ZnTiO_3$@S NCs under natural sunlight irradiation revealed more than 93% destruction of dyes under investigation as a contaminant in 180 min [41]. PAN-based polymers are becoming increasingly popular due to their outstanding spinnability and chemical stability [42, 43].

In the present study, different concentrations of Co(II) TPHPP in chloroacetylated poly(p-hydroxystyrene) were developed and electrospun with varying ratios of PAN to fabricate PAN/(Co(II) TPHPP/CAPS) nanofiber mats coded NF4, NF5, NF6, and NF7. Fabricated mats were examined for green-oxidative degradation of CV dye with H_2O_2 in aqueous solutions. Among these materials, NF6, composed of a 1:1 ratio of PAN to Co(II)TPHPP/CAPS with a lower Co(II) TPHPP loading, demonstrated the highest catalytic activity, decomposing CV completely within 60 min. The influence of H_2O_2, dosage of the catalyst, temperature, and recycling of nanofiber mats were discussed to understand the degradation mechanism of CV and optimize the catalytic degradation system. An interesting finding was the enhanced recovery and recyclability of the catalyst even after five cycles of reuse due to the immobilization of metalloporphyrin on chloroacetylated polymer-supported nanofiber mats.

2 Materials and methods

2.1 Materials

Pyrrole was purchased from Merck, Germany, and distilled before direct usage. 4-Hydroxybenzaldhyde, linear poly(p-hydroxystyrene), polyacrylonitrile (Mwt 150,000 g/mol), crystal violet dye, and Cobalt(II) chloride hexahydrate were obtained from Sigma-Aldrich, Germany. El-Nasr Pharmaceutical Chemicals, Egypt, supplied chloroacetyl chloride, pyridine, propionic acid, chloroform, methylene chloride, methanol, hydrogen peroxide, dimethylformamide, and sodium carbonate. Silica gel (60–120 mesh) was purchased from Fisher Co., New Jersey, USA.

2.2 Synthesis of tetrakis-5, 10, 15, 20 (4-Hydroxyphenyl) porphyrin (TPHPP)

4-Hydroxy benzaldehyde (7.2 mmol) was refluxed in propionic acid (30 mL), then (7.2 mmol) purified pyrrole was added, and the refluxing continued for a further 2 h. the formed precipitated porphyrin was filtrated and washed by chloroform several times, and finally, column chromatography with an eluent 30:1 mixture of methylene chloride and methanol was used for purification [44, 45].

^{1}HNMR (400 MHz, in DMSO): δ (ppm) 10.03 (s,4H, O.H.), 8.9 (s, 8H, βH), 8.03 (d, 8H, ArH), 7.24 (d, 8H, ArH),-2.84 (s, 2H, N.H.) (Fig. S1, *supplementary data*).

2.3 Synthesis of Co(II) TPHPP complex 1

About 0.2 g (0.294 mmol) of TPHPP and 0.3 g (0.294 mmol) Co(II) $Cl_2.6H_2O$ were dissolved in 20 mL methanol under nitrogen air and refluxed for 5 h, then filtered to remove an excess of reactant and the product Co(II) TPHPP **1** was obtained by evaporation the solvent using rotary evaporator [46].

^{1}HNMR (400 MHz, in DMSO): δ (ppm) 10.03 (s,4H, O.H.), 9.13 (s, 8H, βH), 7.9 (d, 8H, ArH), 7.25 (d, 8H, ArH) *(*Fig. S2, *supplementary data).*

2.4 Synthesis of chloroacetylation of linear poly (p-hydroxy styrene) (CAPS)

Pyridine was added to a solution of linear poly (*p*-hydroxy styrene) (66.67 mmol) dissolved in DMF (60 mL). Then, 100.44 mmol of chloroacetyl chloride was added drop-wise under continuous stirring in an iced bath. The mixture was stirred and cooled at standard temperature for three hours and three days. The CAPS (Scheme 1) was precipitated by

pouring in 1N HCl, filtered, and rained many times with distilled water [47].

## 2.5 Synthesis of chloroacetylated polymer supported Co(II) TPHPP

Two different concentrations of **1** (0.068 and 0.027 mmol) were dissolved in DMF, then were added to (1 and 2 g) of chloroacetylated polymer, respectively, with sodium carbonate. The mixtures were stirred for 6 h under N_2 air at 80 °C. Products **2** and **3** were obtained by evaporation of solvent using a rotary and then washed with water several times, and the reaction was shown in Scheme 1 [48].

ICP-MS was used to determine the cobalt (II) content of polymer-supported Co(II) TPHPPs 2 and 3. The amount of Co(II) in the solid catalyst (**2, 3**) was 0.127 and 0.031 mg /L, respectively.

2.6 Fabrication of electrospun PAN/(Co(II)TPHPP/ CAPS) nanofiber mats

The electrospinning technique was used to fabricate the catalyst-loaded-PAN nanofibers. Polyacrylonitrile and (Co(II)

Scheme 1 Chloroacetylated polymer CAPS supported Co(II) TPHPP
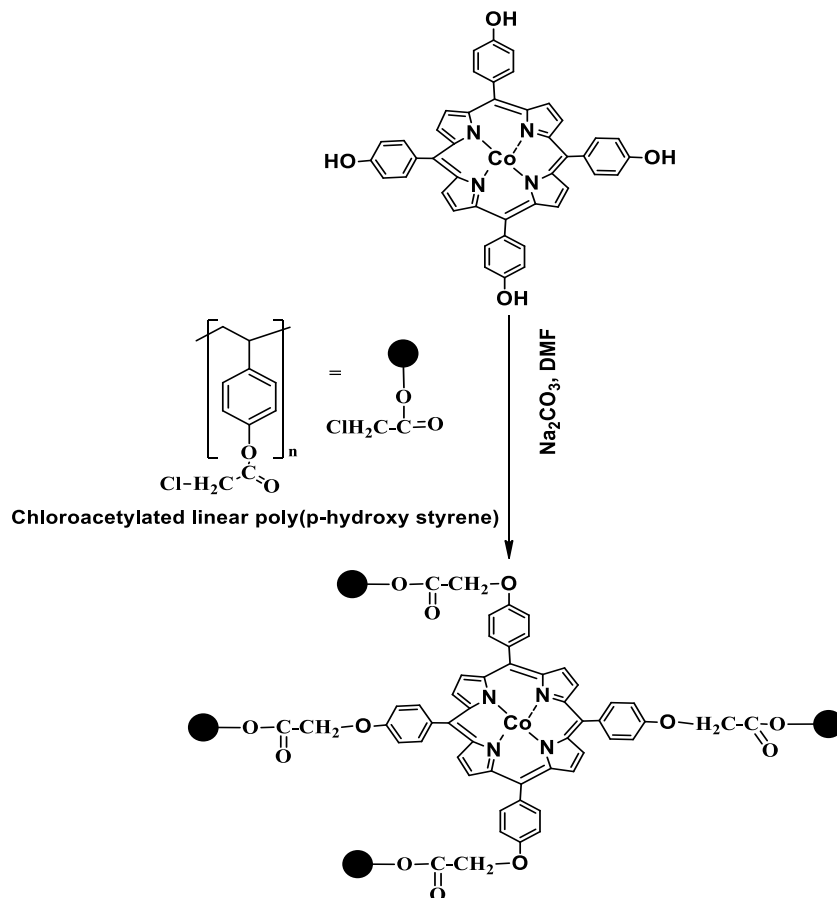
TPHPP/CAPS) 2 and 3 were mixed in DMF in different ratios as PAN and Co(II)TPHPP/CAPS 2 in (1:1 and 2:1) to obtain nanofiber mats NF4 and NF5; respectively and for PAN and Co(II)TPHPP/CAPS 3 in (1:1 and 2:1) to receive nanofiber mats NF6 and NF7; respectively. Then, the mixed solution was placed into a 5 mL syringe (feeding rate: 0.5 mL/h), and the electrospun spacing between the collector and syringe tip was maintained at 10 cm, and voltages were set at 15 kV [49].

2.7 Catalytic degradation of CV using PAN/(Co(II) TPHPP/CAPS) nanofibers NF4-7 by H_2O_2

Crystal violet dye degradation in aqueous media using PAN/(Co(II) TPHPP/CAPS) nanofiber as a catalyst with H_2O_2 was performed as follows: 12 mg of electrospun nanofiber was put in a flask with 10 mL of $(3.9 \times 10^{-5}$ M) CV aqueous solution with initial pH 7, and the solution was stirred at 40 °C. 0.234 M H_2O_2 was added to start the reaction, and UV–visible spectroscopy was used to follow the degradation rate.

At desired time intervals, 3 mL aliquots were taken out of the reaction flask and subjected to analysis. The UV of CV was calculated at wavelengths of 581 nm. The aliquots were then added back to the reaction flask. Pseudo-first order relation was applied to fit the results from destruction results:

$$\ln\left(A_o \backslash A_t\right) = K_{obs}t \tag{1}$$

where A_o is the dye's initial absorbance (at $t = 0$ min), A_t is that absorbance, and K_{obs} (min^{-1}) is the observed rate constant calculated from the slope of the linear plot of ln (A_o/A_t). Each experiment was carried out triplicated ($n = 3$).

2.8 Recycling of the catalyst

Successive catalytic destruction experiments under optimum conditions were achieved to investigate the recycling ability of the catalyst for at least 5 cycles. For these tests, the same nanofiber sample was utilized. The following parameters were set for the experiment: 12 mg catalyst dosage: 10 mL solution volume; initial 3.9×10^{-5} M dye concentration: 0.234 M H_2O_2 concentration at 40 °C and reaction time: 60 min. The nanofiber mat rains with water after each experiment and then reused. The degradation efficiency was investigated according to:

$$\text{Degradation efficiency} \% = [(A_o - A_t)/A_o] \times 100 \tag{2}$$

A_o is the absorbance of dye at zero time, and A_t is the absorbance of dye at time "t," at $\lambda_{max} = 581$ nm.

2.9 Instrumental characterization

UV–VIS: UV–visible spectroscopy was used to measure the absorbance of dye using (Shimadzu 2100-S UV/Vis, Japan) absorption double beam spectrophotometer.

FTIR: Fourier-transform infrared spectroscopy, spectrum data was recorded using a Perkin Elmer 1430 instrument (Massachusetts, USA). The tested samples were scanned at 400–4000 cm^{-1} through absorbance or transmittance mode.

TGA: model (Perkin-Elmer TGA 4000, Germany, was used under nitrogen gas. The platinum pan sample holder was initially closed well, and accurately weighed samples were transferred. The dynamic nitrogen flow rate was 40 ml/min, and the heating rate was 10 °C/min with a temperature range of 32–500 °C.

SEM: a scanning electron microscope (SEM; Model JSM 6360 LA, Joel, Japan) was utilized to examine the morphology of created nanofibers. The nanofibers were coated by Au target through two coating cycles before the investigation.

ICP-MS: The metal concentration of the metalloporphyrin was determined using inductively coupled plasma optical emission spectroscopy using an ICP-OES Spectro-flame model FVMØ3, USA.

^{1}H NMR: Nuclear Magnetic Resonance (NMR) spectra were acquired using (Bruker 400 MHz Avance III NMR spectrometer, Germany) using DMSO-d6 as a solvent.

3 Results and discussion

The free porphyrin TPHPP was prepared by condensing pyrrole and 4-hydroxybenzaldehyde in propionic acid. A metallation of free base porphyrins with cobalt chloride in DMF led to Co(II) TPHPP **1**. Then, Co(II) porphyrin covalently bonded to poly (chloroacetylated hydroxystyrene) was conducted by refluxing in the presence of potassium carbonate, as shown in scheme 1. Finally, polymeric-supported Co(II) porphyrin was electrospuned with PAN as a co-spinning agent and DMF as a solvent, and electrospun spacing between the collector and syringe tip was maintained at 10 cm. Voltages were set at 15 kV, forming nanofiber mats NF[4–7]. The free and metalloporphyrin structures were investigated by UV–visible absorbance. The UV–vis spectra revealed a characteristic strong band (Soret band) at 421 nm and four Q bands around 516, 554, 592, and 650 nm, each less intense for free TPHPP. While, for Co(II) TPHPP, the Soret band was little shifted to 431 nm, and Q bands diminished to two rounds at 543 and 578 nm, as shown in Fig. 1(A, B), which indicated the formation of a metalloporphyrin complex.

3.1 FT-IR analysis

As shown in Fig. 1C, the FTIR spectrum of THPP (a) is consistent with its chemical structure. The stretching vibrations of -O.H. and -N.H. groups showed a broad band at ν 3423 cm^{-1}. Additionally, the peaks at ν 1228 and 1169 cm^{-1}
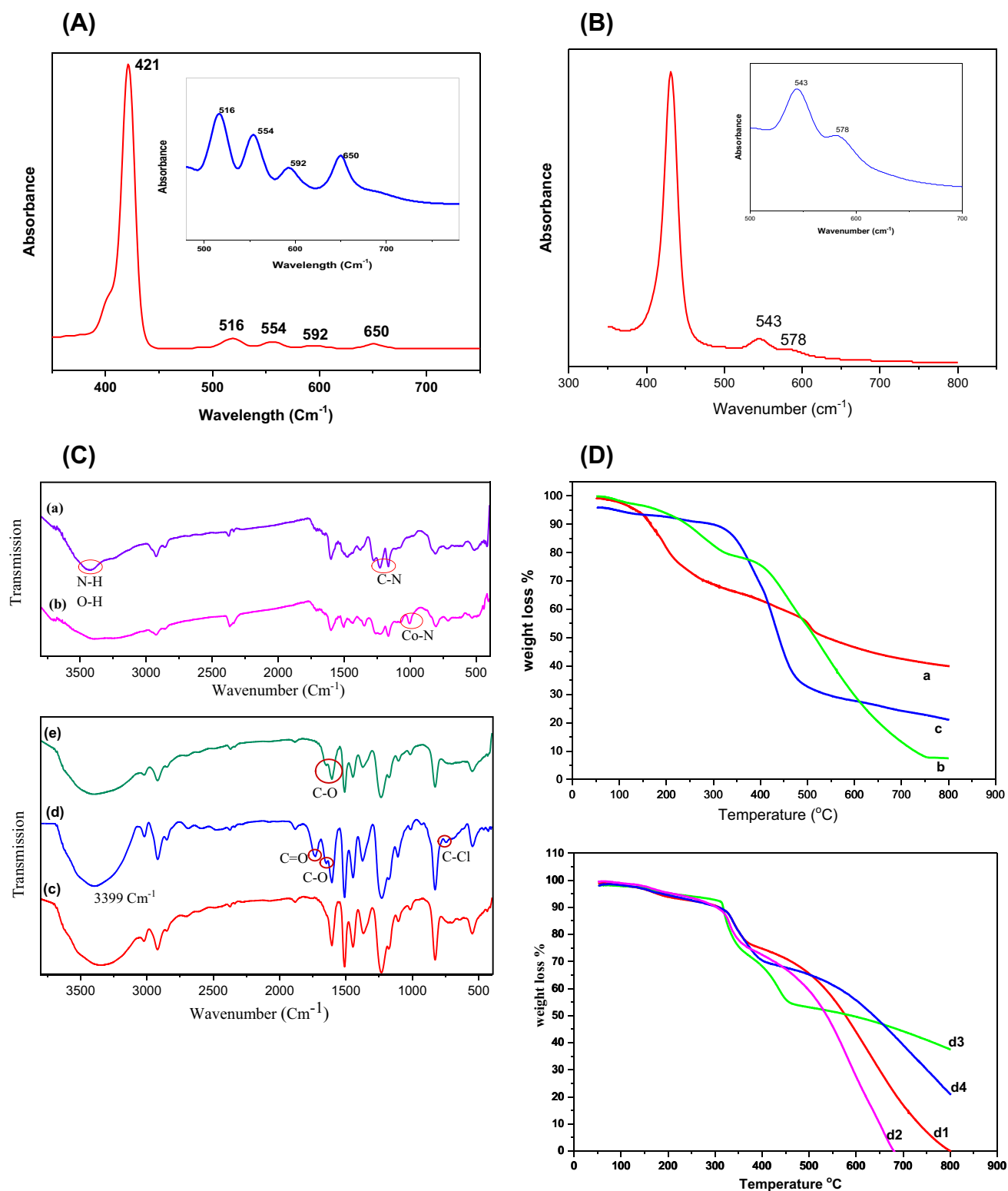
Fig. 1 UV–visible spectra of TPHPP (**A**) and Co(II) TPHPP (**B**), FT-IR spectra (**C**) for TPHPP (a), Co(II) TPHPP (b), linear poly (*p*-hydroxy styrene) (c), CAPs (d), and Co(II)TPHPP/CAPS (e), (**D**) TGA thermographs for (a) TPHPP, (b) Co(II) TPHPP, (c) Co(II)TPHPP/CAPS and (d1) NF4, (d2) NF6, (d3) NF5, (d4) NF7 nanofiber mats

were attributed to C-N stretching vibrations of amine groups, while peaks at ν 1599 and 1469 cm^{-1} were assigned to N–H bending and C=N vibrations, respectively. Finally, the peak at ν 808 cm^{-1} was referred to the macrocycle ring's N–H out-of-plane bending vibration. In the Co(II) THPP spectrum (Fig. 1C-b), the peak at ν 3423 cm^{-1} became broad and slightly shifted. The new peak at ν 1001 cm^{-1} has appeared, which is characteristic absorption of the Co–N$_{(equatorial)}$ bond formed in Co(II) THPP [50].

For the chloroacetylated polymer (Fig. 1C-d), new peaks at ν 1731 and 1656 cm^{-1} indicated the presence of C=O group. Also, a new peak at 743 cm^{-1} confirmed the presence of C–Cl in the chloroacetyl group [47]. For the porphyrin-polymer spectrum (Fig. 1C-e), the broad peak around at ν 3342 cm^{-1} was slightly shifted to ν 3399 cm^{-1}, and the intensity was diminished. Also, the band at ν 1731 cm^{-1} was shifted and interfered with the other bands at ν 1656 and 1611 cm^{-1} due to attaching Co(II) TPHPP to CAPS [51, 52]. The disappearance of the peak at ν 743 cm^{-1} proves that the Co(II) THPP molecules were covalently anchored to the polymer surface. As seen, signature bands for Co(II) TPHPP did not appear anywhere in the spectrum of Co(II) TPHPP/CAPS due to the overlap of the spectra of CAPS and Co(II) THPP in the entire infrared region, which led to the sole appearance of CAPS bands [31, 53].

3.2 TGA results

To study the thermal stability of poly(chloroaceylated styrene) supported Co(II) porphyrin compared to Co(II) porphyrin,

TGA thermographs of free porphyrin, Co(II) porphyrin, and the polymer-reinforced porphyrin were measured and shown in Fig. 1-D. It was demonstrated that Co(II) porphyrin was lower thermal stability than free ligand which may be related to the presence of Co(II) as center metal in the metalloporphyrin, poly(chloroaceylated hydroxy styrene) supported Co(II) porphyrin catalyst showed higher thermal stability than metalloporphyrin (Fig. 1-D), due to its containing on Co(II) as an inorganic constitutes matters in addition synthetic polymer parts, as compared to either pure polymers or porphyrin alone. After porphyrin incorporation onto the surface of the polymer showed a total weight loss of 80%. In comparison, 60% and 93% weight losses are observable in the case of free porphyrin and Co(II) porphyrin, respectively. While NF5 and NF7 showed higher thermal stability than NF4 and NF6, this might be due to the high ratio of PAN in N.F.s that can hinder the thermal decomposition if compared with low PNA contents in N.F.s 4 and 6.

3.3 SEM investigation

Morphologies of electrospun PAN NFs were observed by SEM investigation. Without incorporating PAN as co-spinning, NFs could not be obtained regularly, where beaded N.F.s were formed. Adding PAN into polymer-supported Co(II) porphyrin solution with a ratio (1:1), NFs with few beads were formed with fibers diameter ranging ~106–679 nm, as shown in Fig. 2(a, b). It is observed that, by increasing the concentration of PAN solution to begin (2:1), beads begin to reduce, and fibers' diameter is recorded around ~143–393 nm,

Fig. 2 SEM images of electrospun nanofibers with different ratios of PAN (all images were taken with original magnification×20,000 and scale 4 µm)
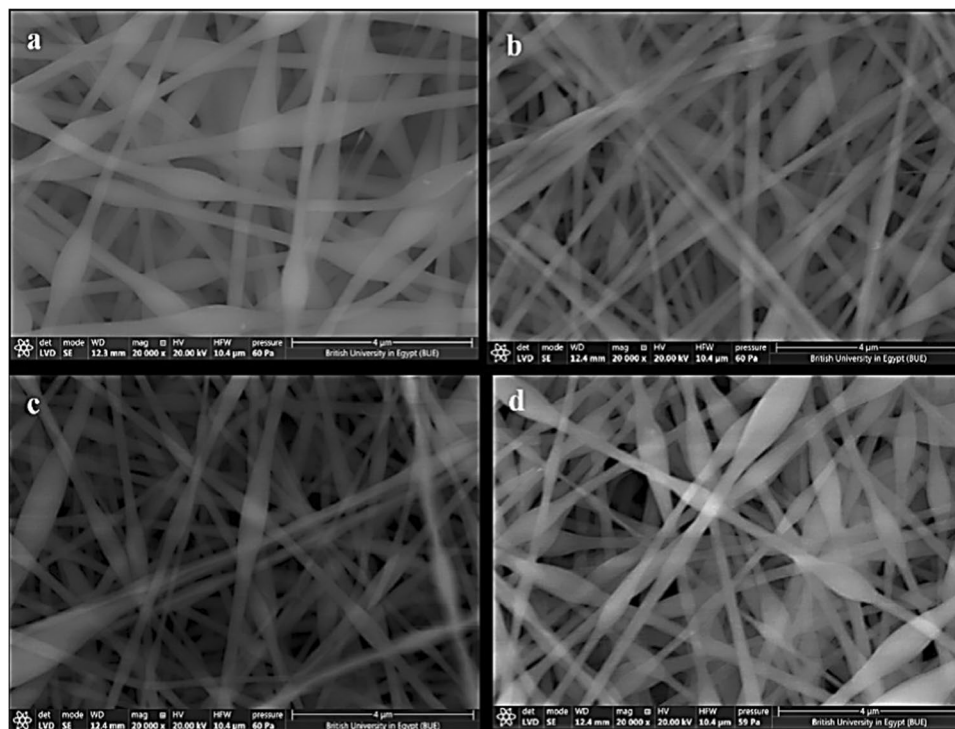
as shown in Fig. 2(c, d). This proves that PAN was used as a co-spinning agent and improved the surface morphology of formed nanofibers, where the surface morphology of fabricated nanofibers was enhanced with increased PAN contents.

3.4 Investigation of the catalytic degradation of crystal violet dye

Catalytic decomposition of CV as a model of organic contamination in aqueous solution was evaluated by applying different ratios of PAN/(Co(II)TPHPP/CAPS) nanofiber NF4-7 with H_2O_2. CV dye had an influential absorption band at $\lambda = 581$ nm, where the decrease of this band indicated degradation of CV. Figure 3A shows the kinetic curve for the destruction of CV; the plot of (lnA_0/A_t) against time presented a straight line, this indicated that the degradation of CV is considered as first-order rate kinetics [54, 55], and it could be described as $\ln A_0/A_t = k_{obs} t$.

Interestingly, all PAN-supported (Co(II)TPHPP/CAPS) nanofibers NF4-7 were displayed as activator catalysts for destroying CV with H_2O_2 in aqueous solutions. Results summarized in Fig. 3A shows that NF6, which is composed of (1: 1 ratio of PAN: Co(II)TPHPP/CAPS) with a less loaded amount of Co(II)TPHPP on the CAPS, was found to be the most effective catalyst for the destruction of CV. These findings might be owing to the increasing of the catalyst dosage of Co(II)TPHPP covalently bonded to the CAPS on nanofiber affects the mass transfer rates of H_2O_2 and CV in the solution bulk that could lead to a decrease in the degradation efficiency [56]. Figure 3B presents the change of the absorbance of CV with time using H_2O_2 and NF6. It could be observed that the main absorbance band at λ 581 nm almost vanished, and the degradation percent of CV reached 98% in 60 min. H_2O_2 and Co(II)TPHPP present in NF**6** played an essential role in the degradation of CV, as illustrated
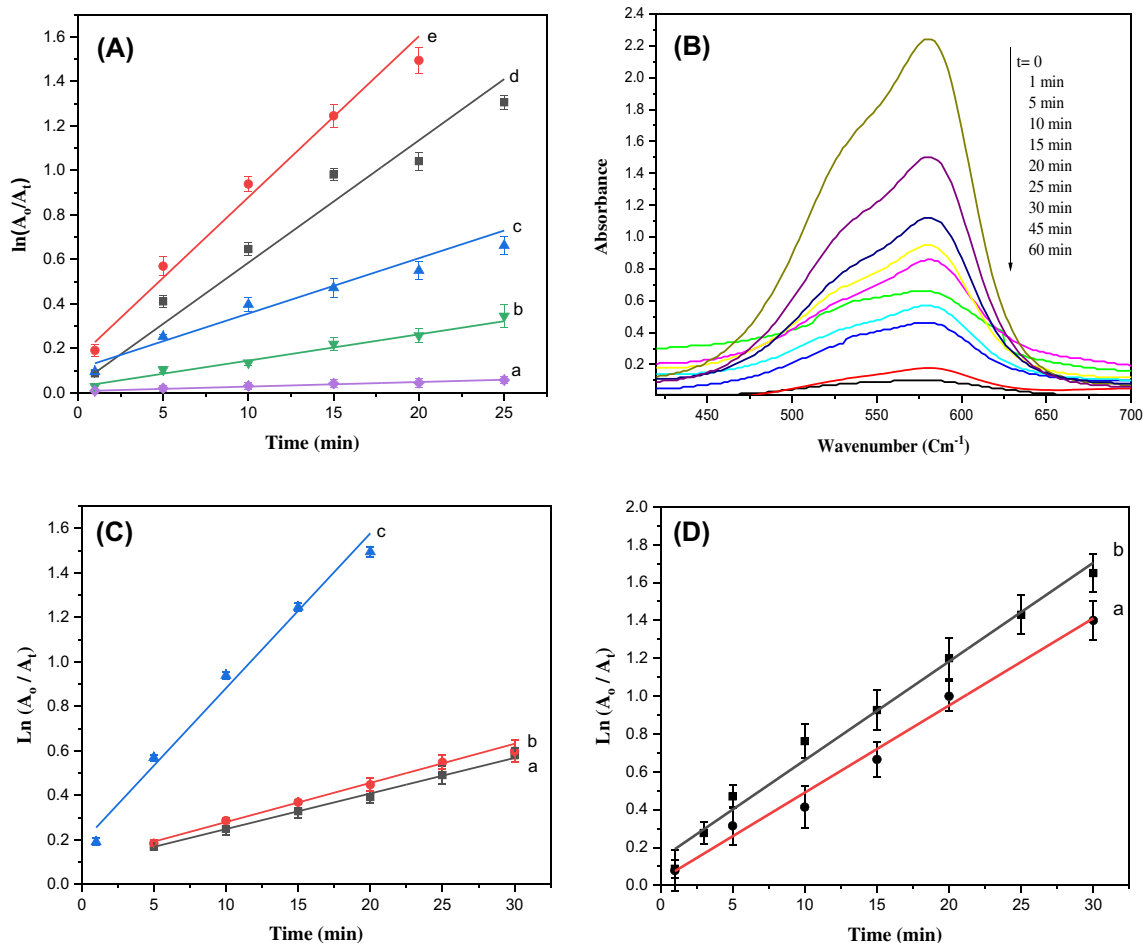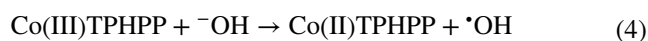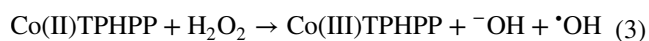

Fig. 3 A Catalytic degradation rate of CV dye (a) without catalyst and in the presence of nanofiber catalysts, (b) NF4, (c) NF5, (d) NF7, and (e) NF6. **B** UV–VIS spectra of CV degradation using NF6 with H_2O_2 as the function of time. Catalyst 6: 12 mg; [CV]: (3.9×10^{-5} M, [H_2O_2]: 0.234 M, pH:5.5 at 40 °C). **C** The rate of degradation of CV dye in the presence of PAN\CAPS nanofiber with H_2O_2 (a), PAN\ (Co(II)TPHPP\CAPS) nanofiber without H_2O_2 (b), and PAN\(Co(II) TPHPP\CAPS) nanofiber with H_2O_2 (c). **D** The degradation rate of CV dye using (a) Co(II) TPHPP/CAPS, (b) PAN/(Co(II) TPHPP/ CAPS) nanofiber (SD mean, $n = 3$)

in Fig. 3C. It showed that the rate of degradation of CV in the presence of PAN/poly (chloroaceylated hydroxy styrene) nanofiber with H_2O_2 was the same as in fact of PAN\(Co(II)TPHPP/CAPS) nanofiber without H_2O_2. The degradation rate may be attributed to the adsorption of the CV on the surface of PAN/poly (chloroaceylated styrene) nanofiber.

In contrast, in the case of NF6 with H_2O_2, the degradation rate was seven times faster, as shown in Fig. 3C. Hydroxyl radicals ($^{\bullet}OH$) generated as shown in (Eqs. 3, 4, 5) from Co(II) porphyrin and H_2O_2 according to the Fenton-like response [20, 57, 58] are a better oxidant (reducing potential is 2.07 V at pH ~ 7) which accelerate the oxidation and destruction of organic contamination such as azo dyes [59]. In supported Fenton-like reactions, the catalyst surface typically formed $^{\bullet}OH$ radicals, and the degrading process was considered a surface-mediated operation [57].

$$Co(II)TPHPP + H_2O_2 \rightarrow Co(III)TPHPP + {}^{-}OH + {}^{\bullet}OH \quad (3)$$

$$Co(III)TPHPP + {}^{-}OH \rightarrow Co(II)TPHPP + {}^{\bullet}OH \quad (4)$$

$$CV + {}^{\bullet}OH \rightarrow Product \quad (5)$$

Catalytic degradation of CV was also investigated in the presence/absence of a PAN nanofiber mat. Figure 3D shows that both Co(II) TPHPP/CAPS and PAN/Co(II) TPHPP/CAPS NF6 degraded CV, indicating that Co(II) TPHPP species is the key factor to influence the degradation efficiency and rate of the reaction due to the formation of $^{\bullet}OH$ radicals with H_2O_2. The significant acceleration in the presence of PAN in NF6 must be supposedly owing to the higher surface area of NF6, which led to the best diffusion of the metalloporphyrin polymer particles homogeneously [60].

The effect of the concentration of H_2O_2, dosage of catalyst, and temperature of the medium on the catalytic degradation of CV using PAN/(Co(II) TPHPP/CAPS) nanofiber 6 as catalyst and H_2O_2 was investigated in detail.
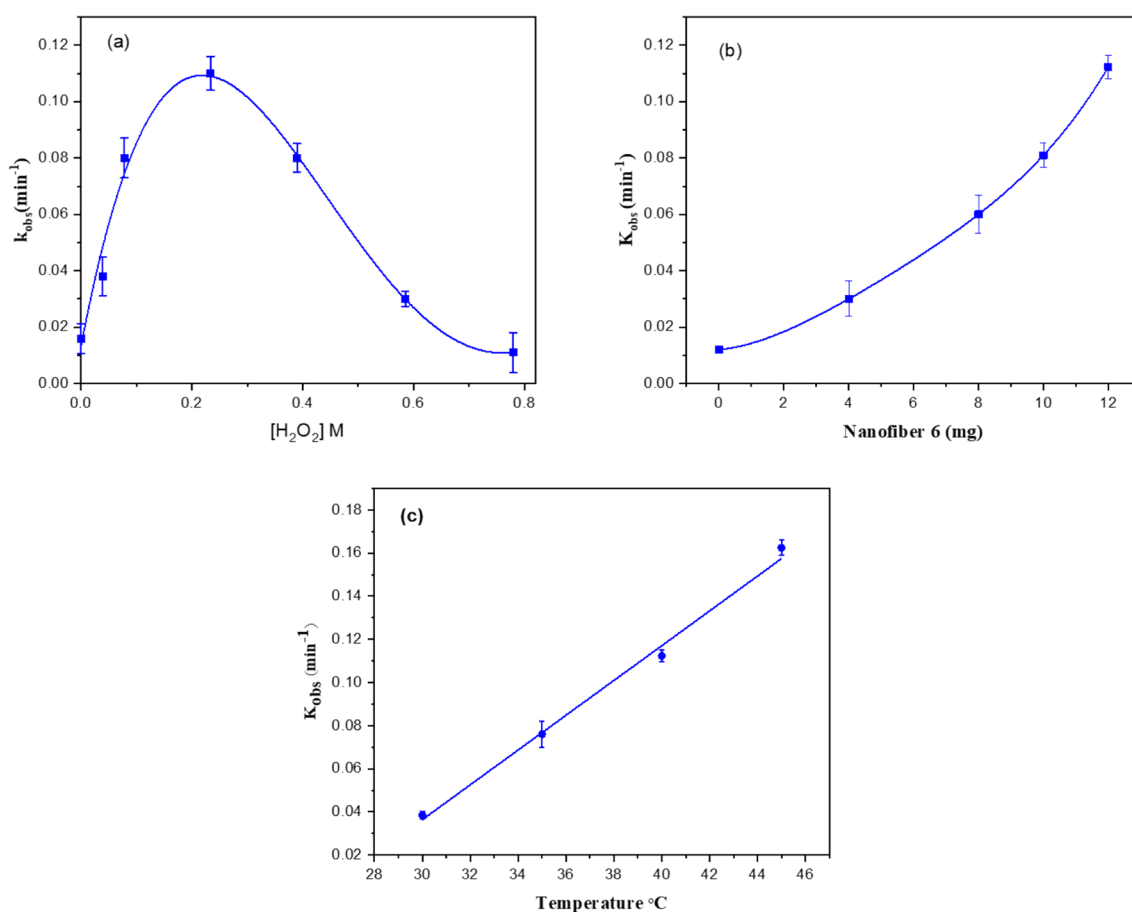

Fig. 4 **a** Influence of H_2O_2 concentration on the rate of degradation of CV by PAN/(Co(II) TPHPP/CAPS) nanofiber 6. Catalyst 6: 12 mg; CV: 3.9×10^{-5} M, pH:5.5 at 40 °C, **b** influence of catalyst dosage on the oxidative degradation rate of CV dye. [CV]: 3.9×10^{-5} M; [H_2O_2]: 0.234 M, pH:5.5 at 40 °C, and **c** effect of solution temperature on the catalytic degradation of CV by NF6. Catalyst 6: 12 mg; [CV]: 3.9×10^{-5} M, [H_2O_2]: 0.234 M, pH:5.5, (SD mean, $n = 3$)

Table 1 Rate constant and activation parameters of catalytic degradation of CV by NF6 with H_2O_2

Temperature (K)	K_{obs} (min^{-1})	E (kJ mol^{-1})	$\Delta H^{\#}$ (kJ mol^{-1})	$\Delta G^{\#}$ (kJ mol^{-1})	$\Delta S^{\#}$ (J mol^{-1} K^{-1})
303	0.03825	80.44	77.86	21.35	181.97
308	0.0755				
313	0.11236				
318	0.16251				

Table 2 Recycling activity NF6

Recycled times	Reaction time (min)	Degraded CV (%)
First	60	88.3
Second	60	89.2
Third	60	87.3
Fourth	60	87.7
Fifth	60	87.2

3.4.1 Effect of H_2O_2 concentration on the degradation process

Figure 4(a) illustrates the influence of the concentration of H_2O_2 on the oxidative rate of CV. The rate observed was raised with increasing the concentration of H_2O_2 as shown in Fig. 4a, and then declined when the amount of H_2O_2 increased, which, owing to Further increase in the concentration of H_2O_2 partly inhibited the oxidation rate due to the well-known hydroxyl radicals scavenging effect. Reaction occurred between the reactive species ˙OH radical and H_2O_2 to form the approximately stable peroxyl radical $HO_2^{\bullet}$ radical, considered less active compared with ● OH

radical as shown in Eq. (6, 7) [61]. The undesirable reactions (6) and (7) competed with destroying the dye chromophore. These reactions reduced the probability of attacking the CV molecules by hydroxyl radicals, which decreased the degradation rate of the dye at a high concentration of H_2O_2. Thus, a hydrogen peroxide with a concentration of 0.234 M was chosen for the degradation of CV to achieve high degradation efficiency.

$$H_2O_2 + {}^{\bullet}OH \rightarrow HO_2{}^{\bullet} \tag{6}$$

$$HO_2{}^{\bullet} + {}^{\bullet}OH \rightarrow H_2O + O_2 \tag{7}$$

3.4.2 Effect of nanofiber dosage

To illustrate the effect of nanofiber dosage on the degradation of CV by PAN/(Co(II) TPHPP/CAPS) NF6, experiments were performed at various catalyst dosages, as shown in Fig. 4b. It was noticed that the oxidation rate was raised by increasing the catalyst mass of NF6 from 4 to 12 mg. This is affiliated with the increasing number of active sites on electrospun nanofiber particles, generating more hydroxyl radicals. Accordingly, radicals' raised attainability enhanced the CV solution's degradation [62].
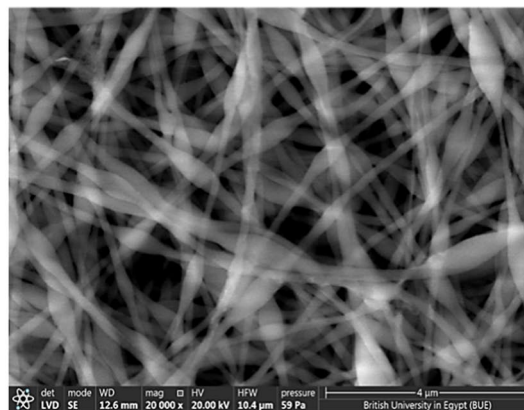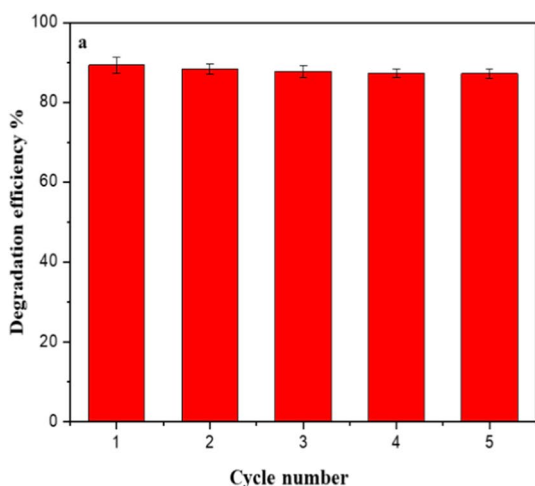

Fig. 5 **a** Effect of NF6 recycling on the degradation of CV dye (SD mean, $n = 3$). Catalyst 6: 12 mg; [CV]: 3.9×10^{-5} M, [H_2O_2]: 0.234 M, pH:5.5 at 40 °C, and **b** SEM image of NF6 after passing recycling (original magnification×20,000 and scale 4 µm)

3.4.3 Effect of temperature

The change in reaction medium temperature significantly influences the rate of chemical reactions [63, 64]. The influence of temperature variation on the breakdown of CV by NF6 with H_2O_2 was investigated. Figure 4c illustrates that the degradation rate was raised gradually by raising the solution temperature from 30 to 45 °C. Two acceptable illustrations for that are first, migration of CV from the reaction medium to nanofiber accelerated or secondly, production of a reactive surface species or the activation energy $\Delta G^{\#}$ raised as the temperature elevated [65]. $\Delta G^{\#}$ was calculated from the diagram of ln k_{obs} against 1/T. The chart was linear with a high correlation coefficient R^2 (0.992), and the values of activation factors are shown in Table 1. $\Delta H^{\#}$ and $\Delta G^{\#}$ had positive values, indicating the catalytic reaction's endothermic and nonspontaneous nature. In contrast, the higher value of $\Delta S^{\#}$ showed the presence of a highly ordered transition state.

3.4.4 Recycling of the catalyst

Heterogonous catalysts played a significant role in reducing reaction costs, minimizing waste generation, and leading more environmentally and economically saving methods for separation and recycling [36]. PAN-supported (Co(II) TPHPP/CAPS) NF6 was readily reused from the solution by simple filtration and recycled for successive reactions after being rained several times with water. Degradation percentages of CV were illustrated in Table 2 and Fig. 5a for the recycled NF6. No suggestive changes were detected after five successive cycles of the NF6. These data were compatible with similar SEM images for the freshly synthesized and reused PAN/(Co(II) TPHPP/CAPS) NF6, as in Fig. 5b.

4 Conclusion

In conclusion, new efficient nanofiber mats supported catalysts were developed by immobilizing different concentrations of Co(II) TPHPP in chloroacetylated poly(*p*-hydroxy styrene) and then electrospun with different ratio of PAN to form PAN/(Co(II) TPHPP/CAPS) nanofiber mats NF4-7. NFs were examined effectively as a heterogeneous activator for green-oxidative destruction of CV dye with H_2O_2. Interestingly, all NF4-7 showed highly efficient catalysts for the breakdown of CV, whereas NF6 with a less loaded amount of Co(II)TPHPP on the CAPS seems to be the most effective catalyst for the oxidation of CV, where CV almost vanished after 60 min. The effect of H_2O_2 concentration, catalyst dosage, and medium temperature on the oxidative degradation of CV using NF6 as a catalyst was investigated in detail. The most effective economic issue was the catalyst's enhanced recovery and recyclability due to the immobilization of metalloporphyrin on chloroacetylated

polymer-supported nanofiber mats. Remarkably, even after five cycles of reuse, there was no significant degradation in the catalytic activity of the recycled catalyst. This breakthrough highlights the potential of these materials in addressing water pollution challenges efficiently and sustainably.

Declarations

Ethical approval Not applicable.

Competing interests The authors declare no competing interests.

References

1. Mota HP, Quadrado RF, Iglesias BA, Fajardo AR (2020) Enhanced photocatalytic degradation of organic pollutants mediated by Zn (II)-porphyrin/poly (acrylic acid) hybrid microparticles. Appl Catal B: Environ 277:119208. https://doi.org/10.1016/j.apcatb.2020.119208

2. Wang CC, Li JR, Lv XL, Zhang YQ, Guo G (2014) Photocatalytic organic pollutants degradation in metal–organic frameworks. Energy Environ Sci 7(9):2831–2867. https://doi.org/10.1039/C4EE01299B

3. Ucoski GM, Machado GS, de Freitas Silva G, Nunes FS, Wypych F, Nakagaki S (2015) Heterogeneous oxidation of the dye Brilliant Green with H_2O_2 catalyzed by supported manganese porphyrins. J Mol Catal A Chem 408:123–131. https://doi.org/10.1016/j.molcata.2015.07.020

4. Rashed MN (2013) Adsorption technique for the removal of organic pollutants from water and wastewater. Organ Pollut-Monit Risk Treat 7:167–194

5. Saha TK, Frauendorf H, John M, Dechert S, Meyer F (2013) Efficient oxidative degradation of azo dyes by a water-soluble manganese porphyrin catalyst. ChemCatChem 53:796–805. https://doi.org/10.1002/cctc.201200475

6. Mittal J, Ahmad R, Ejaz MO, Mariyam A, Mittal A (2022) A novel, eco-friendly bio-nanocomposite (Alg-Cst/Kal) for the adsorptive removal of crystal violet dye from its aqueous solutions. Int J Phytoremediation 24(8):796–807. https://doi.org/10.1080/15226514.2021.1977778

7. Kassem KO, Hussein MA, Motawea MM, Gomaa H, Alrowaili Z, Ezzeldien M (2021) Design of mesoporous ZnO@ silica fume-derived SiO_2 nanocomposite as photocatalyst for efficient crystal violet removal: effective route to recycle industrial waste. J Clean Prod 326:129416. https://doi.org/10.1016/j.jclepro.2021.129416

8. Gomaa H, Abd El-Monaem EM, Eltaweil AS, Omer AM (2022) Efficient removal of noxious methylene blue and crystal violet dyes at neutral conditions by reusable montmorillonite/$NiFe_2O_4$@ amine-functionalized chitosan composite. Sci Rep 12(1):15499. https://doi.org/10.1038/s41598-022-19570-1

9. Ahmed M, Abou-Gamra Z, Medien H, Hamza M (2017) Effect of porphyrin on photocatalytic activity of TiO_2 nanoparticles toward Rhodamine B photodegradation. J Photochem Photobiol B Biol 176:25–35. https://doi.org/10.1016/j.jphotobiol.2017.09.016

10. La DD, Tran CV, Hoang NT, Ngoc MDD, Nguyen TP, Vo HT et al (2020) Efficient photocatalysis of organic dyes under simulated sunlight irradiation by a novel magnetic $CuFe_2O_4$@ porphyrin nanofiber hybrid material fabricated via self-assembly. Fuel 281:118655. https://doi.org/10.1016/j.fuel.2020.118655

11. Vo HT, Nguyen AT, Tran CV, Nguyen SX, Tung NT, Pham DT et al (2021) Self-assembly of porphyrin nanofibers on ZnO nanoparticles for the enhanced photocatalytic performance for organic dye degradation. ACS Omega 6(36):23203–23210. https://doi.org/10.1021/acsomega.1c02808

12. Hassanein M, Gerges S, Abdo M, El-Khalafy S (2005) Catalytic activity and stability of anionic and cationic water soluble cobalt (II) tetraarylporphyrin complexes in the oxidation of 2-mercaptoethanol by molecular oxygen. J Mol Catal A Chem 240(1–2):22–26. https://doi.org/10.1016/j.molcata.2005.05.043

13. Zeng HQ, Jiang Q, Zhu YF, Yan XH, Liang XB, Hu HY et al (2006) Catalysis of metalloporphyrins for selective hydroxylation of phenol by H_2O_2. J Porphyr Phthalocyanines 10(02):96–103. https://doi.org/10.1142/S1088424606000120

14. El-Khalafy SH, Hassanein M (2012) Oxidation of 2-aminophenol with molecular oxygen and hydrogen peroxide catalyzed by water soluble metalloporphyrins. J Mol Catal A Chem 363:148–152. https://doi.org/10.1016/j.molcata.2012.06.002

15. Che CM, Lo VKY, Zhou CY, Huang JS (2011) Selective functionalisation of saturated C-H bonds with metalloporphyrin catalysts. Chem Soc Rev 40(4):1950–1975. https://doi.org/10.1039/C0CS00142B

16. Lu H, Zhang XP (2011) Catalytic C-H functionalization by metalloporphyrins: recent developments and future directions. Chem Soc Rev 40(4):1899–1909. https://doi.org/10.1039/C0CS00070A

17. Serra AC, Docal C, Gonsalves ADAR (2005) Efficient azo dye degradation by hydrogen peroxide oxidation with metalloporphyrins as catalysts. J Mol Catal A Chem 238(1–2):192–198. https://doi.org/10.1016/j.molcata.2005.05.017

18. Emmert FL III, Thomas J, Hon B, Gengenbach AJ (2008) Metalloporphyrin catalyzed oxidation of methyl yellow and related azo compounds. Inorganica Chim Acta 361(8):2243–2251. https://doi.org/10.1016/j.ica.2007.09.048

19. Xu A, Li X, Ye S, Yin G, Zeng Q (2011) Catalyzed oxidative degradation of methylene blue by in situ generated cobalt (II)-bicarbonate complexes with hydrogen peroxide. Appl Catal B: Environ 102(1–2):37–43. https://doi.org/10.1016/j.apcatb.2010.11.022

20. El-Khalafy S, Hassanein M, Abd-Elal M, Atia A (2020) Oxidation of azo dye Orange II with hydrogen peroxide catalyzed by 5, 10, 15, 20-tetrakis [4-(diethylmethylammonio) phenyl] porphyrinato-cobalt (II) tetraiodide in aqueous solution. J Saudi Chem Soc 24(7):520–526. https://doi.org/10.1016/j.jscs.2020.05.003

21. Silvestri S, Fajardo AR, Iglesias BA (2021) Supported porphyrins for the photocatalytic degradation of organic contaminants in water: a review. Environ Chem Lett 1–41. https://doi.org/10.1007/s10311-021-01344-2

22. Bizaia N, de Faria EH, Ricci GP, Calefi PS, Nassar EJ, Castro KA et al (2009) Porphyrin− kaolinite as efficient catalyst for oxidation reactions. ACS Appl Mater Interfaces 1(11):2667–2678. https://doi.org/10.1021/am900556b

23. Barros VP, Faria AL, MacLeod TC, Moraes LA, Assis MD (2008) Ironporphyrin immobilized onto montmorillonite as a biomimetical model for azo dye oxidation. Int Biodeterior Biodegrad 61(4):337–344. https://doi.org/10.1016/j.ibiod.2007.10.008

24. Zucca P, Vinci C, Sollai F, Rescigno A, Sanjust E (2008) Degradation of Alizarin Red S under mild experimental conditions by immobilized 5, 10, 15, 20-tetrakis (4-sulfonatophenyl) porphine–Mn (III) as a biomimetic peroxidase-like catalyst. J Mol Catal A Chem 288(1–2):97–102. https://doi.org/10.1016/j.molcata.2008.04.001

25. Shen C, Song S, Zang L, Kang X, Wen Y, Liu W et al (2010) Efficient removal of dyes in water using chitosan microsphere supported cobalt (II) tetrasulfophthalocyanine with H_2O_2. J Hazard Mater 177(1–3):560–566. https://doi.org/10.1016/j.jhazmat.2009.12.069

26. Zucca P, Vinci C, Rescigno A, Dumitriu E, Sanjust E (2010) Is the bleaching of phenosafranine by hydrogen peroxide oxidation catalyzed by silica-supported 5, 10, 15, 20-tetrakis-(sulfonatophenyl) porphine-Mn (III) really biomimetic? J Mol Catal A Chem 321(1–2):27–33. https://doi.org/10.1016/j.molcata.2010.01.015

27. Chen Z, Wang T, Jin X, Chen Z, Megharaj M, Naidu R (2013) Multifunctional kaolinite-supported nanoscale zero-valent iron used for the adsorption and degradation of crystal violet in aqueous solution. J Colloid Interface Sci 398:59–66. https://doi.org/10.1016/j.jcis.2013.02.020

28. Nishimoto R, Zhu Q, Miyamoto T, Sato T, Tu X, Aneksampant A et al (2015) Monopersulfate oxidation of Acid Orange 7 with an iron (III)-tetrakis (N-methylpyridinium-4-yl) porphyrin intercalated into the layers of montmorillonite and pillared clay. J Mol Catal A Chem 396:84–89. https://doi.org/10.1016/j.molcata.2014.09.035

29. Rayati S, Sheybanifard Z (2016) Catalytic activity of Mn (III) and Fe (III) porphyrins supported onto multi-walled carbon nanotubes in the green oxidation of organic dyes with hydrogen peroxide: a comparative study. J Iran Chem Soc 3(3):541–546. https://doi.org/10.1007/s13738-015-0763-0

30. Krishnakumar B, Balakrishna A, Arranja CT, Dias CM, Sobral AJ (2017) Chemically modified amino porphyrin/TiO2 for the degradation of Acid Black 1 under day light illumination. Spectrochim Acta A Mol Biomol Spectrosc 176:134–141. https://doi.org/10.1016/j.saa.2017.01.019

31. Mota HP, Quadrado RF, Burgo TA, Iglesias BA, Fajardo AR (2020) Polysaccharide/Fe (III)-porphyrin hybrid film as catalyst for oxidative decolorization of toxic azo dyes: an approach for wastewater treatment. Arab J Chem 13(7):5923–5938. https://doi.org/10.1016/j.arabjc.2020.04.021

32. Trocha A, Impert O, Katafias A, van Eldik R (2021) Mechanistic details of the catalytic degradation of methylene blue by hydrogen peroxide in basic solution. The unexpected innocence of percarbonate. Polyhedron 210:115507. https://doi.org/10.1016/j.poly.2021.115507

33. Nie G, Li Z, Lu X, Lei J, Zhang C, Wang C (2013) Fabrication of polyacrylonitrile/CuS composite nanofibers and their recycled application in catalysis for dye degradation. Appl Surf Sci 284:595–600. https://doi.org/10.1016/j.apsusc.2013.07.139

34. Shao L, Hu B, Dong P, Ji W, Qi C (2010) Electrospinning Fe (III) porphyrin/TiO_2/poly (styrene) mixture: formation of a novel nanofiber photocatalyst for the photodegradation of methyl orange. J Porphyr Phthalocyanines 14(11):993–999. https://doi.org/10.1142/S1088424610002823

35. Yan S, Zhan NQ, Miao Y, Yang QB, Zhang CQ, Wang HG et al (2008) Fabrication of poly (4-vinylpyridine) nanofiber and fluorescent poly (4-vinylpyridine)/porphyrin nanofiber by electrospinning. Chem Res Chin Univ 24(6):722–725. https://doi.org/10.1016/S1005-9040(09)60014-3

36. Ognibene G, Gangemi CM, D'Urso A, Purrello R, Cicala G, Fragalà ME (2018) Combined approach to remove and fast detect heavy metals in water based on PES–TiO₂ electrospun mats and porphyrin chemosensors. ACS Omega 3(7):7182–7190. https://doi.org/10.1021/acsomega.8b00284

37. Huang J, Wang D, Hou H, You T (2008) Electrospun palladium nanoparticle-loaded carbon nanofibers and their electrocatalytic activities towards hydrogen peroxide and NADH. Adv Funct Mater 18(3):441–448. https://doi.org/10.1002/adfm.200700729

38. Shao L, Xing G, Lv W, Yu H, Qiu M, Zhang XM et al (2013) Photodegradation of azo-dyes in aqueous solution by polyacrylonitrile nanofiber mat-supported metalloporphyrins. Polym Int 62(2):289–294. https://doi.org/10.1002/pi.4298

39. Rahmat M, Rehman A, Rahmat S, Bhatti HN, Iqbal M, Khan WS et al (2019) Highly efficient removal of crystal violet dye from water by MnO₂ based nanofibrous mesh/photocatalytic process. J Mater Res Technol 8(6):5149–5159. https://doi.org/10.1016/j.jmrt.2019.08.038

40. Vinosel VM, Anand S, Janifer MA, Pauline S, Dhanavel S, Praveena P et al (2019) Enhanced photocatalytic activity of Fe₃O₄/SnO₂ magnetic nanocomposite for the degradation of organic dye. J Mater Sci Mater Electron 30(10):9663–9677. https://doi.org/10.1007/s10854-019-01300-5

41. Tavakoli-Azar T, Mahjoub AR, Sadjadi MS, Farhadyar N, Sadr MH (2020) Improving the photocatalytic performance of a perovskite ZnTiO3 through ZnTiO₃@ S nanocomposites for degradation of Crystal violet and Rhodamine B pollutants under sunlight. Inorg Chem Commun 119:108091. https://doi.org/10.1016/j.inoche.2020.108091

42. Fallahi D, Rafizadeh M, Mohammadi N, Vahidi B (2008) Effect of applied voltage on jet electric current and flow rate in electrospinning of polyacrylonitrile solutions. Polym Int 57(12):1363–1368. https://doi.org/10.1002/pi.2482

43. Shao L, Liu J, Ye Y, Zhang XM, Qi C (2011) Polyacrylonitrile fiber mat-supported palladium catalyst for Mizoroki-Heck reaction in aqueous solution. Appl Organomet Chem 25(9):699–703. https://doi.org/10.1002/aoc.1830

44. Rojkiewicz M, Kuś P, Kozub P, Kempa M (2013) The synthesis of new potential photosensitizers. Part 2. Tetrakis-(hydroxyphenyl) porphyrins with long alkyl chain in the molecule. Dyes Pigm 99(3):627–635. https://doi.org/10.1016/j.dyepig.2013.06.029

45. Fadda AA, El-Mekawy RE, El-Shafei A, Freeman HS, Hinks D, El-Fedawy M (2013) Design, synthesis, and pharmacological screening of novel porphyrin derivatives. J Chem 2013. https://doi.org/10.1155/2013/340230

46. Gómez-Vidales V, Borja-Miranda A, Cortez-Maya S, Amelines-Sarria O, Rivera M, Martínez-García M (2016) Design and synthesis of a multi Cu (II)-porphyrin array. Open Chem J 3(1). https://doi.org/10.2174/1874842201603010025

47. Kenawy ER, Abdel-Hay F, El-Newehy M, Abd El-Zaher EH, Abo-Elghit IEM (2016) Novel biocidal polymers based on branched and linear poly (hydroxystyrene). Int J Polym Mater Polym Biomater 65(14):712–719. https://doi.org/10.1080/00914037.2016.1163563

48. Yu XQ, Huang JS, Yu WY, Che CM (2000) Polymer-supported ruthenium porphyrins: versatile and robust epoxidation catalysts with unusual selectivity. J Am Chem Soc 122(22):5337–5342. https://doi.org/10.1021/ja000461k

49. Arai T, Tanaka M, Kawakami H (2012) Porphyrin-containing electrospun nanofibers: positional control of porphyrin molecules in nanofibers and their catalytic application. ACS Appl Mater Interfaces 4(10):5453–5457. https://doi.org/10.1021/am3013664

50. Wang R, Jiao W, Gao B (2009) Efficient biomimetic aerobic oxidation of phenylethane catalyzed by P (4VP-co-St)/SiO₂-supported metalloporphyrins. Appl Surf Sci 255(17):7766–7772. https://doi.org/10.1016/j.apsusc.2009.04.166

51. Rayati S, Rezaie S, Nejabat F (2018) Mn (III)-porphyrin/graphene oxide nanocomposite as an efficient catalyst for the aerobic oxidation of hydrocarbons. C R Chim 21(7):696–703. https://doi.org/10.1016/j.crci.2018.03.003

52. Khojastehnezhad A, Bakavoli M, Javid A, KhakzadSiuki MM, Moeinpour F (2019) Covalently copper (II) porphyrin cross-linked graphene oxide: preparation and catalytic activity. Catal Lett 149:713–722. https://doi.org/10.1007/s10562-019-02665-2

53. Ghoochani SH, Heshmati A, Hosseini HA, Darroudi M (2022) Adsorption and photocatalytic properties of porphyrin loaded MIL-101 (Cr) in methylene blue degradation. Environ Sci Pollut Res 29(23):34406–34418. https://doi.org/10.1007/s11356-022-18640-1

54. Sobana N, Swaminathan M (2007) Combination effect of ZnO and activated carbon for solar assisted photocatalytic degradation of Direct Blue 53. Sol Energy Mater Sol Cells 91(8):727–734. https://doi.org/10.1016/j.solmat.2006.12.013

55. Li X, Cheng Y, Kang S, Mu J (2010) Preparation and enhanced visible light-driven catalytic activity of ZnO microrods sensitized by porphyrin heteroaggregate. Appl Surf Sci 256(22):6705–6709. https://doi.org/10.1016/j.apsusc.2010.04.074

56. Fang ZD, Zhang K, Liu J, Fan JY, Zhao ZW (2017) Fenton-like oxidation of azo dye in aqueous solution using magnetic Fe₃O₄-MnO₂ nanocomposites as catalysts. Water Sci Eng 10(4):326–333. https://doi.org/10.1016/j.wse.2017.10.005

57. Chen Y, Pötschke P, Pionteck J, Voit B, Qi H (2019) Fe₃O₄ nanoparticles grown on cellulose/G.O. hydrogels as advanced catalytic materials for the heterogeneous Fenton-like reaction. ACS Omega 4(3):5117–25. https://doi.org/10.1021/acsomega.9b00170

58. Turrà N, Neuenschwander U, Baiker A, Peeters J, Hermans I (2010) Mechanism of the catalytic deperoxidation of tert-butylhydroperoxide with cobalt (II) acetylacetonate. Chem Eur J 16(44):13226–13235. https://doi.org/10.1002/chem.201000489

59. Ahmed Y, Yaakob Z, Akhtar P (2016) Degradation and mineralization of methylene blue using a heterogeneous photo-Fenton catalyst under visible and solar light irradiation. Catal Sci Technol 6(4):1222–1232. https://doi.org/10.1039/C5CY01494H

60. Wan LS, Wu J, Xu ZK (2006) Porphyrinated nanofibers via copolymerization and electrospinning. Macromol Rapid Commun 27(18):1533–1538. https://doi.org/10.1002/marc.200600381

61. Chan K, Chu W (2005) Atrazine removal by catalytic oxidation processes with or without U.V. irradiation: Part I—quantification and rate enhancement via kinetic study. Appl Catal B: Environ 58(3–4):157–163. https://doi.org/10.1016/j.apcatb.2004.12.005

62. Kaliannan D, Palaninaicker S, Velayutham P, Palanivel V, Kumar AJ (2018) Novel synthesis of Chrysanthemum indicum flower as an adsorbent for the removal of direct Congo red from aqueous solution. Desalin Water Treat 113:270–280. https://doi.org/10.5004/dwt.2018.22292

63. Reardon EJ, Fagan R, Vogan JL, Przepiora A (2008) Anaerobic corrosion reaction kinetics of nanosized iron. Environ Sci Technol 42(7):2420–2425. https://doi.org/10.1021/es0712120

64. Zhang Z, Cissoko N, Wo J, Xu X (2009) Factors influencing the dechlorination of 2, 4-dichlorophenol by Ni–Fe nanoparticles in the presence of humic acid. J Hazard Mater 165(1–3):78–86. https://doi.org/10.1016/j.jhazmat.2008.09.080

65. Faria AL, Mac Leod TC, Assis MD (2008) Carbamazepine oxidation catalyzed by iron and manganese porphyrins supported on aminofunctionalized matrices. Catal Today 133:863–869. https://doi.org/10.1016/j.cattod.2007.12.022